Journal of Ceramic Processing Research. Vol. 17, No. 7, pp. 707~711 (2016)

J O U R N A L O F
Ceramic Processing Research

Mechanical properties and rapid sintering of binderless nanostructured TiC and WC by high frequency induction heated sintering

In-Jin Shon*

Division of Advanced Materials Engineering, the Research Center of Hydrogen Fuel Cell, Chonbuk National University, 664-14 Deokjin-dong 1-ga, Deokjin-gu, Jeonju, Jeonbuk 561-756, Korea

The rapid sintering of nanostructured TiC and WC hard materials in a short time was investigated with high-frequency induction heating sintering process. The advantage of this process is that it allows very quick densification to near theoretical density and prohibition of grain growth in nanostructured materials. A dense nanostructured TiC and WC hard material with a relative density of up to 99% was produced with simultaneous application of 80 MPa pressure and induced current of output of total power capacity (15 kW) within one min. The sintering behavior, grain size and mechanical properties of binderless TiC and WC were investigated.

Key words: Sintering, Powder metallurgy, Nanostructured materials, Fracture toughness, Hardness.

Introduction

Several attractive properties associated with transition metal carbides, such as WC, TaC, NbC and TiC, have prompted numerous investigations on the synthesis and processing of these carbides as single phase materials and as composites with metallic phases. The attractive properties of these carbides are high melting temperature, high hardness, high thermal and electrical conductivities, and a relatively high chemical stability. These carbides find applications primarily in the cutting tool industries. In this regard, they are used as cemented carbides in which the carbides are in combination with a binder metal, such as Co or Ni. Of the four carbides given above as examples, WC is the most important in the cemented carbide application. It has a high melting point (a peritectic melting temperature of 2785 °C) and high hardness (16 ~ 22 GPa Vickers at 500 g load) [1, 2]. In more recent studies, WC has been suggested for other uses, for example as a catalyst substituting for noble metals (Pt, Ir, and Pd) [3-5]. Other recent applications of WC that have been reported include its use as catalyst electrode in fuel cells and as a coating for aerospace components [6]. Cemented carbide is usually prepared by sintering WC powder with a cobalt binder by means of conventional sintering techniques at temperatures near the melting point of cobalt. Considering the high melting point of WC, it is obviously difficult to sinter WC without Co or another low-melting point binder using a conventional process in which the liquid phase is partly necessary during the sintering process [7].

TiC is also very stable, with a melting temperature of 3430 K, and does not undergo phase transformations. These properties have seen it used extensively in cutting tool and abrasive materials in composite with a binder metal, such as Ni. But, these binder phases of Ni and Co have inferior chemical characteristics to the carbide phase. Most notably, corrosion and oxidation occurs preferentially in the binder phase [8]. Hence, the development of binderless TiC and WC is needed to apply in mechanical seals and sliding parts due to its enhanced corrosion resistance.

As nanomaterials possess high strength, high hardness, excellent ductility and toughness, undoubtedly, more attention has been paid for the application of nanomaterials [9, 10]. In recent days, nanocrystalline powders have been developed by the thermochemical and thermomechanical process named as the spray conversion process (SCP), co-precipitation and high energy milling [11-13]. However, the grain size in sintered materials becomes much larger than that in pre-sintered powders due to a fast grain growth during conventional sintering process. Therefore, even though the initial particle size is less than 100 nm, the grain size increases rapidly up to 500 nm or larger during the conventional sintering [14]. So, controlling grain growth during sintering is one of the keys to the commercial success of nanostructured materials. In this regard, the high frequency induction heated sintering method (HFIHS) which can make dense materials within 2 minutes has been shown to be effective in achieving this goal [15-18].

In this work, we investigated the sintering of TiC and WC without the use of a binder by the HFIHS method. The goal of this research is to produce dense fine

*Corresponding author:
Tel : +82-63-270-2381
Fax: +82-63-270-2386
E-mail: ijshon@chonbuk.ac.kr

grained binderless TiC and WC hard materials. In addition, we also studied the sintering behavior, microstructure and mechanical properties of binderless TiC and WC.

Experimental Procedure

The titanium carbide powder with a grain size of < 2 mm and 99.5% purity used in this research was supplied by Alfa. The tungsten carbide powder with a grain size of < 0.5 mm and 99.8% purity used in this research was supplied by Taegu Tec. These powders were first milled in a high-energy ball mill (Pulverisette-5 planetary mill) at 250 rpm for 10 h. Tungsten carbide balls (9 mm in diameter) were used in a sealed cylindrical stainless steel vial under an argon atmosphere. The weight ratio of balls-to-powder was 30 : 1. Milling resulted in a significant reduction of the grain size. The grain sizes of the TiC and WC were calculated from the full width at half-maximum (FWHM) of the diffraction peak by Suryanarayana and Norton's formula [19]:

$$B_r(B_{crystalline} + B_{strain})\cos\theta = k\lambda/L + \eta\sin\theta \quad (1)$$

where B_r is the full width at half-maximum (FWHM) of the diffraction peak after instrument correction; $B_{crystalline}$ and B_{strain} are FWHM caused by small grain size and internal stress, respectively; k is constant (with a value of 0.9); λ is wavelength of the X-ray radiation; L and η are grain size and internal strain, respectively; and θ is the Bragg angle. The parameters B and B_r follow Cauchy's form with the relationship: $B = B_r + B_s$, where B and B_s are FWHM of the broadened Bragg peaks and the standard sample's Bragg peaks, respectively.

The powders were placed in a graphite die (outside diameter, 35 mm; inside diameter, 10 mm; height, 40 mm) and then introduced into the high-frequency induction heating sintering (HFIHS) apparatus shown schematically in Fig. 1. The HFIHS apparatus includes a 15 kW power supply which provides an induced current through the sample, and 50 kN uniaxial press. The system was first evacuated and a uniaxial pressure of 80 MPa was applied. An induced current was then activated and maintained until the densification rate was negligible, as indicated by real-time output of the shrinkage of the sample. The shrinkage was measured by a linear gauge measuring the vertical displacement. The HFIHS can be controlled in two ways: by temperature control or by output control. The latter was chosen. The output level was 80% output of total power. Temperatures were measured by a pyrometer focused on the surface of the graphite die. At the end of the process, the induced current was turned off and the sample cooled to room temperature. The process was carried out under a vacuum of 5.33 Pa.

The relative density of the sintered sample was measured by the Archimedes method. Microstructural information was obtained from product samples, which had been polished and etched using Murakami's reagent (10 g potassium ferricyanide, 10 g NaOH, and 100 ml water) for 1 ~ 2 min at room temperature. Compositional and microstructural analyses of the products were made through X-ray diffraction (XRD), scanning electron microscopy (SEM) with energy dispersive spectroscopy (EDS) and field emission scanning electron microscope (FE-SEM). Vickers hardness was measured by performing indentations at a load of 20 kg_f and a dwell time of 15 s.

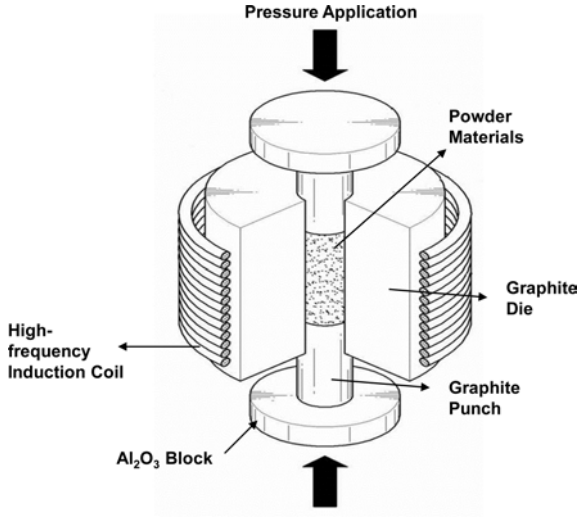

Fig. 1. Schematic diagram of the high-frequency induction heating sintering apparatus.

Results and Discussion

Fig. 2 shows X-ray diffraction patterns of the TiC and WC powders after milling for 10 h. The full width at half-maximum (FWHM) of the diffraction peak is wider with milling time due to strain and refinement of powder. The powder sizes of TiC and WC milled for 10 h were 24 and 11 nm, respectively using Suryanarayana and Norton's formula [19]. SEM images of TiC and WC powders with milling for 10 h are shown in Fig. 3. TiC and WC powders have irregular shape and refinement with milling time. The variations of the shrinkage displacement and temperature with the heating time for 80% of the total output power capacity (15 kW) during the sintering of the high energy ball milled TiC and WC powders under a pressure of 80 MPa are shown in Fig. 4. In all cases, as the induced current was applied, thermal expansion showed up to 1200 °C. And then shrinkage displacement rapidly increased due to consolidation. High-energy ball milling treatment allows the control of the formation of compound by fixing the reactant powder microstructure. Indeed, high-energy ball milling produces finer crystallites, strain and defects. Therefore, consolidation temperature decreases with

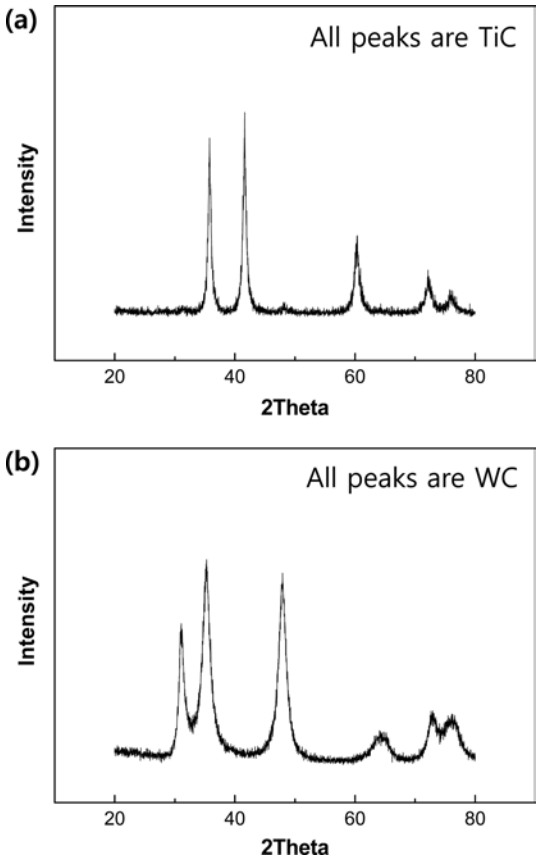

Fig. 2. X-ray diffraction patterns of the (a) TiC and (b) WC powders after milling for 10 h.

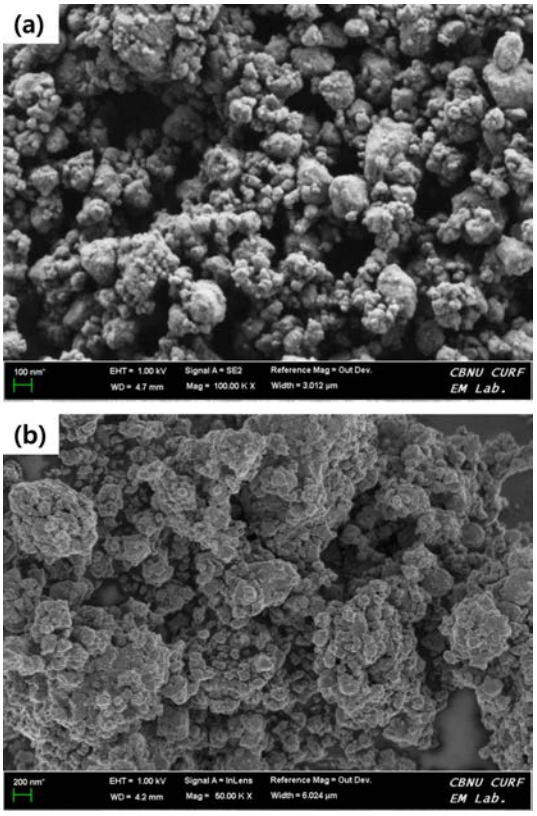

Fig. 3. SEM images of the (a) TiC and (b) WC powders with milling for 10 h.

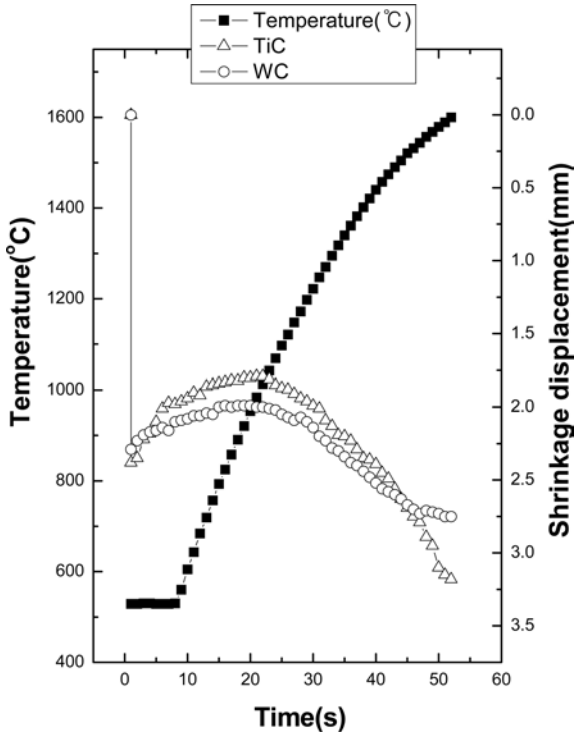

Fig. 4. Variations of temperature and shrinkage with heating time during the sintering of binderless TiC and WC powders with milling for 10 h.

milling time because driving force for sintering and contact points of powders for atomic diffusion increases. Fig. 5 shows the XRD patterns of TiC and WC sintered by high frequency induction heating. All peaks are TiC and WC, respectively. Plots of $B_r(B_{crystalline}+B_{strain})$ cosè versus sinè in Suryanarayana and Norton's formula are shown in Fig. 6. The average grain sizes of the TiC and WC calculated from the XRD data were about 162 and 44 nm, respectively and their corresponding densities were approximately 99 and 97%, respectively. Thus, the average grain size of the sintered TiC and WC is not greatly larger than that of the initial powder, indicating the absence of great grain growth during sintering. This retention of the grain size is attributed to the high heating rate and the relatively short term exposure of the powders to the high temperature. Fig. 7 shows FE-SEM image of TiC and WC sintered from milled powders. The microstuctures of TiC and WC consist of nano-grains. The grain size of TiC is larger than that of WC. It is considered that grain boundary energy of TiC is greater than that of WC.

The role of the current (resistive or inductive) in sintering and or synthesis has been focus of several attempts aimed at providing an explanation to the observed enhancement of sintering and the improved characteristics of the products. The role played by the current has been variously interpreted, the effect being explained in terms of fast heating rate due to Joule heating, the presence of plasma in pores separating

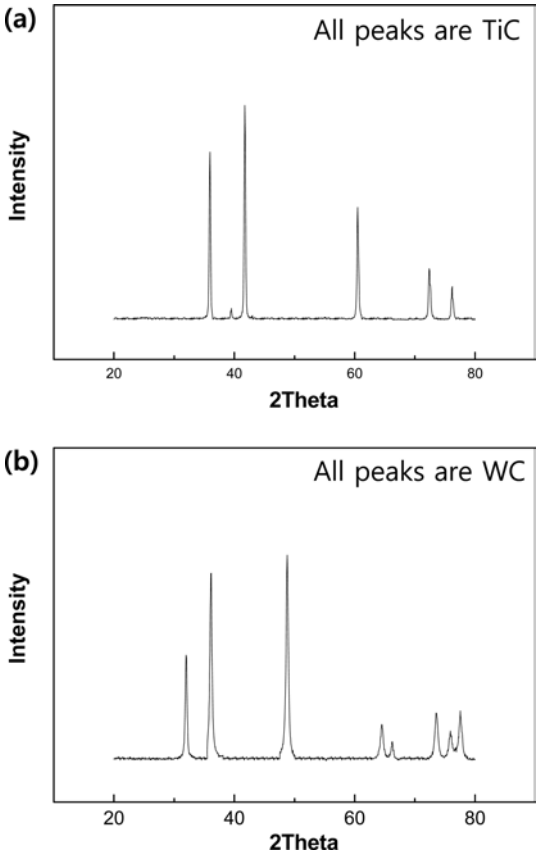

Fig. 5. XRD patterns of binderless (a) TiC and (b) WC sintered from milled powders for 10 h.

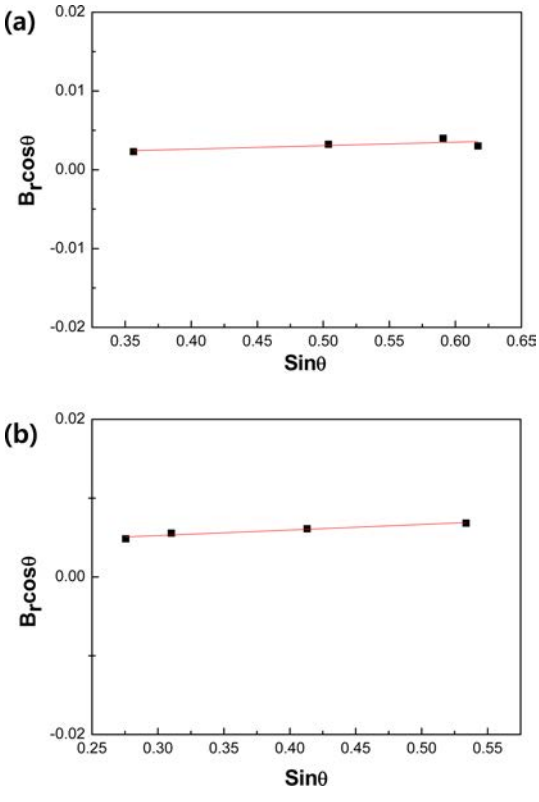

Fig. 6. Plot of B_r ($B_{crystalline} + B_{strain}$) cosθ versus sinθ for (a) TiC and (b) WC sintered from milled powders.

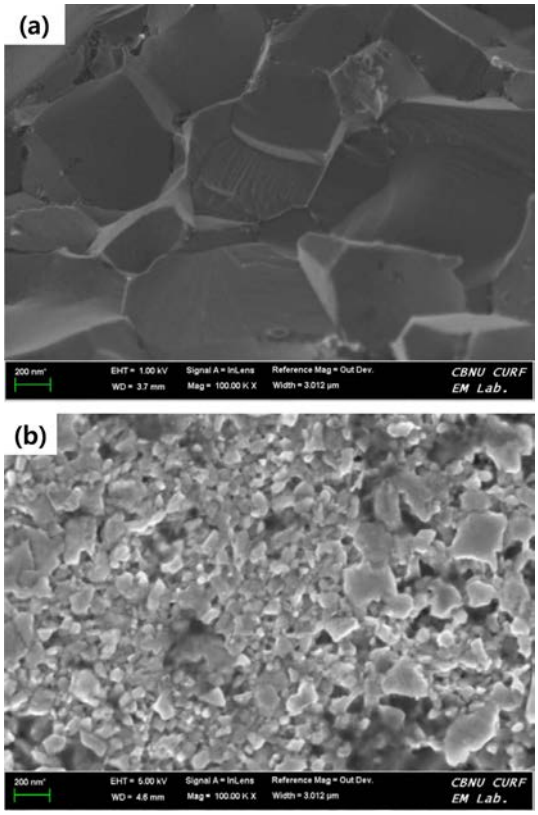

Fig. 7. FE-SEM micrographs of binderless (a) TiC and (b) WC sintered from milled powders.

powder particles [20], and the intrinsic contribution of the current to mass transport [21-23].

Vickers hardness measurements were performed on polished sections of the TiC and WC samples using a 20 kg_f load and 15 s dwell time. Indentations with large enough loads produced radial cracks emanating from the corners of the indent. The length of these cracks permits the fracture toughness of the material to be estimated using Anstis' expression [24],

$$K_{IC}=0.016\ (E/H)^{1/2} \cdot P/C^{3/2} \quad (2)$$

where E is Young's modulus, H is the indentation hardness, P is the indentation load, and C is the trace length of the crack measured from the center of the indentation.

The Vickers hardnesses of the TiC and WC are 2194 and 2800 kg/mm^2, respectively. And their fracture toughnesses were 4.1 and 6.1 $MPa \cdot m^{1/2}$, respectively. These values represent the average of ten measurements. The hardness and fracture toughness of WC are higher than those of TiC due to refinement of grain.

TiC powder could be synthesized by self-propagating high temperature synthesis (SHS) [25], mechanical alloying (MA) [26, 27] and electrothermal combustion [28]. The use of plasma activated sintering to successfully consolidate mechanically alloyed TiC powder has been demonstrated by M. S. El-Eskandarany [27]. The

mechanically synthesized nanopowder of TiC with an average grain size of 5 nm was consolidated at 1963 K for 5 minutes under a pressure of 38.2 MPa to a fully dense nanocrystalline TiC with an average grain size of 60 nm. Comparing the above study with ours, the sintering temperature and time of the high frequency induction heated sintering is lower and shorter than those of plasma activated sintering. The hardness (32 GPa) of TiC studied by M. S. El-Eskandarany is higher than that of ours due to refinement of grain size.

Conclusions

Nanopowders of TiC and WC were made by high energy ball milling. Using the new rapid sintering method, HFIHS, the densification of binderless TiC and WC was accomplished. The average grain sizes of the TiC and WC calculated from the XRD data were about 162 and 44 nm, respectively and their corresponding densities were approximately 99 and 97%, respectively. The Vickers hardnesses of the TiC and WC are 2194 and 2800 kg/mm^2, respectively. And their fracture toughnesses were 4.1 and 6.1 $MPa \cdot m^{1/2}$, respectively. The hardness and fracture toughness of WC are higher than those of TiC due to refinement of grain.

Acknowledgments

This work was supported by a grant in aid awarded by the Basic Research Project of the Korea Institute of Geoscience and Mineral Resources (KIGAM), funded by the Ministry of Science, ICT and Future Planning (GP2015036) and this work was supported by the Korea Institute of Energy Technology Evaluation and Planning (KETEP) and the Ministry of Trade, Industry & Energy (MOTIE) of the Republic of Korea (No. 20164030201070).

References

1. P. Schwartzkopf, and R. Kieffer, Refractory hard metals-boride, carbide, nitride and silicide, MacMillan, New York, 1953.
2. L.E. Toth, Transition metal carbides and nitrides, Academic Press, New York, 1971.
3. L. Leclercq, M. Provost, H. Pastor, G. Grimblot, A.M. Hardy, and L. Gengembre, J. Catalysis 117 (1989) 371-383.
4. M.J. Ledoux, C.H. Pham, J. Guille, and H. Dunlop, J. Catalysis 134 (1992) 383-398.
5. L. Volpe, and M. Boudart, J. Solid State Chem. 59 (1985) 348-356.
6. R. Koc, and S.K. Kodambaka, J. Eur. Ceram. Soc. 20 (2000) 1859-1869.
7. A. Hirata, H. Zheng, and M. Yoshikawa, Diamond and Related Materials 7 (1998) 1669-1674.
8. H. Suzuki et al., Cemented carbide and sintered hard materials, Maruzen, Tokyo, 1986.
9. H.G. Jo, and I.J. Shon, Journal of Ceramic Processing Research 15[6] (2014) 371-375.
10. S.M. Kwon, N.R. Park, J.W. Shin, S.H. Oh, B.S. Kim, I.J. Shon, Korean J. Met. Mater. 53 (2015) 555-562.
11. I.J. Shon, H.S. Kang, J.M. Doh, J.K. Yoon, Met. Mater. Int. 21 (2015) 345-349.
12. B.R. Kang, I.J. Shon, Korean J. Met. Mater. 53 (2015) 320-325.
13. I.J. Shon, Korean J. Met. Mater. 52 (2014) 573-580.
14. M. Sommer, W.D. Schubert, E. Zobetz, and P. Warbichler, Int. J. Refract. Met. Hard Mater. 20 (2002) 41-50.
15. Bo-Ram Kang, Jin-kook Yoon, Kyung-Tae Hong, and In-Jin Shon, Met. Mater. Int., 21(2015) 698-703.
16. I.J. Shon, H.G. Jo, B.S. Kim, J.K. Yoon, and K.T. Hong, Korean J. Met. Mater. 53 (2015) 474-479.
17. In-Jin Shon, Hyoung-Gon Jo, and Hanjung Kwon, Korean J. Met. Mater. 52 (2014) 343-346.
18. Hyun Su Kang, Jung Mann Doh, Jin Kook Yoon, and In Jin Shon, Korean J. Met. Mater. 52 (2014) 759-764.
19. C. Suryanarayana, and M. Grant Norton, X-ray diffraction: a practical approach, Plenum Press, New York, 1998.
20. Z. Shen, M. Johnsson, Z. Zhao, and M. Nygren, J. Am. Ceram. Soc. 85 (2002) 1921-1927.
21. J.E. Garay, U. Anselmi-Tamburini, Z.A. Munir, S.C. Glade, and P. Asoka-Kumar, Appl. Phys. Lett. 85 (2004) 573-575.
22. J.R. Friedman, J.E. Garay. U. Anselmi-Tamburini, and Z.A. Munir, Intermetallics 12 (2004) 589-597.
23. J.E. Garay, U. Anselmi-Tamburini, and Z.A. Munir, Acta Mater. 51 (2003) 4487-4495.
24. G.R. Anstis, P. Chantikul, B.R. Lawn, and D.B. Marshall, J. Am. Ceram. Soc. 64 (1981) 533-538.
25. S.K. Mishra, S. Das, R.P. Goel, and P. Ramachandrarao, J. Mater. Sci. Lett. 16 (1997) 965-967.
26. Q. Yuan, Y. Zheng, and H. Yu, Int. J. Refract. Met. Hard Mater. 27 (2009) 696-700.
27. M. Sherif El-Eskandarany, J. Alloys Compd. 305 (2000) 225-238.
28. I.J. Shon, and Z.A. Munir, J. Am. Ceram. Soc. 81 (1998) 3243-3248.